

Thermoelectric transport properties of Floquet multi-Weyl semimetals

Tanay Nag ¹, Anirudha Menon ², and Banasri Basu³

¹*SISSA, via Bonomea 265, 34136 Trieste, Italy*

²*Department of Physics, University of California, Davis, California 95616, USA*

³*Physics and Applied Mathematics Unit, Indian Statistical Institute, Kolkata 700108, India*



(Received 24 March 2020; accepted 22 June 2020; published 13 July 2020)

We discuss the circularly polarized light (of amplitude A_0 and frequency ω) driven thermoelectric transport properties of type-I and type-II multi-Weyl semimetals (mWSMs) in the high-frequency limit. Considering the low-energy model, we employ the Floquet-Kubo formalism to compute the thermal Hall and Nernst conductivities for both types of mWSMs. We show that the anisotropic nature of the dispersion for arbitrary integer monopole charge $n > 1$ plays an important role in determining the effective Fermi surface behavior; interestingly, one can observe momentum-dependent corrections in Floquet mWSMs in addition to the momentum-independent contribution as observed for Floquet single WSMs. Apart from the nontrivial tuning of the Weyl node position $\pm Q \rightarrow \pm Q - A_0^n/\omega$, our study reveals that the momentum-independent terms result in leading order contributions in the conductivity tensor. This has the form of n times the single-WSM results with effective chemical potential $\mu \rightarrow \mu - A_0^n/\omega$. On the other hand, momentum-dependent corrections lead to subleading order terms which are an algebraic function of μ and are present for $n > 1$. Remarkably, this analysis further allows us to distinguish type-I mWSMs from their type-II counterparts. For type-II mWSMs, we find that the transport coefficients for $n \geq 2$ exhibit an algebraic dependence on the momentum cutoff in addition to the weak logarithmic dependence as noticed for $n = 1$ WSMs. We demonstrate the variation and qualitative differences of transport coefficients between type-I and type-II mWSM as a function of external driving parameter ω .

DOI: [10.1103/PhysRevB.102.014307](https://doi.org/10.1103/PhysRevB.102.014307)

I. INTRODUCTION

Recent years have witnessed Weyl semimetals (WSMs) as a focus of research attraction due to their exotic properties. The upsurge of recent attention on this new class of quantum materials is due to its unusual Fermi arc surface states and chiral anomaly that is intimately related to topological order [1,2]. In WSMs, the bulk band gap closes at an even number of discrete points in the Brillouin zone. These special gap closing points, protected by some crystalline symmetry, are referred as Weyl nodes [3]; Weyl nodes act as a monopoles or antimonopoles of Berry curvature characterized by integer monopole charge n . Two Weyl nodes of different chirality are located at different momenta when the system breaks the time-reversal symmetry; four Weyl nodes are noticed in general for systems with broken inversion symmetry only [2,4]. Moreover, inversion breaking may also lead to the energy-separated Weyl points while time-reversal-symmetry breaking can result in Weyl points at the same energy [5,6]. The existence of Fermi arc surface states, chiral-anomaly-related negative magnetoresistance, and the quantum anomalous Hall effect is the direct consequence of the topological nature of WSMs [7–9]. As compared to the conventional WSMs with $n = 1$, reported in TaP, TaAs, and NbAs [10–12], it has been recently shown that n can be generically greater than 1, with the crystalline symmetries bounding its maximum value to 3 [13–15]. These are called multi-WSMs (mWSMs); interestingly, the single WSM with $n = 1$ can be considered as a 3D analog of graphene whereas the double WSM (triple WSM)

with $n = 2$ ($n = 3$) can be represented as a 3D counterpart of bilayer (ABC -stacked trilayer) graphene [16–18]. Close to the Weyl points, mWSMs host low-energy quasiparticles with the dispersion which is, in general, linear only in one direction leading to anomalous features in the transport properties [19–25].

An ideal WSM has a conical spectrum and a pointlike Fermi surface at the Weyl point. An interesting situation arises when large tilting of the Weyl cones results in a Lifshitz transition. This leads to a new class of materials called type-II WSMs, where the Fermi surface is no longer pointlike [2,26–30]. The existence of type-II WSMs has been experimentally demonstrated [31,32], while theoretical prediction shows that a type-II WSM can be engineered by applying strain or chemical doping to the original type-I WSM [33]. The type-II WSM phase is characterized by a different class of Weyl fermions manifesting the violation of Lorentz symmetry. Type-II WSMs can yield intriguing electronic transport properties due to a markedly different density of states at the Fermi level [34–37]. In addition to electric transport, thermal responses also carry signatures of the exotic physics of WSMs which have been studied theoretically [38–41] and experimentally [42–45]. At the same time, optical conductivity of WSMs has been extensively studied along with other characteristic signatures [46–51]. While much progress has been made experimentally and theoretically in investigating $n = 1$ type-I and type-II WSMs, the experimental discovery of mWSMs with $n \geq 2$ is yet to be made; however, using density functional theory calculations some materials are con-

jected to host Weyl nodes with monopole charges $n = 2, 3$ [13,14,52,53]. This further motivates the theoretical search for finding additional tools to identify these exotic phases with higher monopole charge. For example, mWSMs, in general, can exhibit a smoothly deformed conical spectrum and a pointlike Fermi surface at the Weyl point. Interestingly, for type-II mWSMs, these features are expected to change and might lead to distinct transport characteristics as compared to type-I mWSMs.

On the other hand, periodically driven Floquet systems, where the static Hamiltonian is perturbed with a time-periodic drive, have attracted a great deal of interest recently. Floquet systems can host unique phases which have no counterparts in equilibrium systems, such as anomalous Floquet topological phases [48,54–60], dynamical freezing [61], many-body energy localization [62], dynamical localization [63,64], Floquet higher-order topological phases [65], and dynamical generation of edge Majorana modes [66]. It has been shown that circularly polarized light can be employed to switch between Weyl semimetal, Dirac semimetal, and topological insulator phases in a prototypical three-dimensional (3D) Dirac material, Na_3Bi [67]. Furthermore, the DC transport is expected to be drastically modified under such irradiation [55,68]. Interestingly, linearly polarized light can lead a band insulator to a WSM phase where the relative separation of Weyl points can be controlled [69]; similarly, circularly polarized light drives nodal line semimetals into Weyl semimetals [70]. In the high-frequency driving limit, the system does not absorb energy via electronic transitions, resulting in a nonequilibrium steady state. In this limit, an effective static Sarnath-space Hamiltonian picture successfully describes the nontrivial outcomes [71,72].

Given the background on the generation and optical manipulation of Weyl nodes, our aim here is to study the thermoelectric transport properties of mWSMs when it is driven by a circularly polarized source in the high-frequency limit. The irradiation can act differently depending on whether the underlying static system obeys or breaks the time-reversal symmetry [54,69]. For example, the irradiated graphene, which is intrinsically time-reversal invariant, becomes topologically gapped whereas light-induced WSMs, which can be intrinsically time-reversal broken, remain gapless with renormalized Weyl node position. A recent study using nonequilibrium Kubo formalism has revealed that the thermoelectric response of type-I WSMs can be distinguished from type-II WSMs under the application of light [30]. One can hence note that in mWSMs, the anisotropic dispersion may lead to unusual outcome as compared to the single WSMs and graphene. It is natural to ask the question, ‘‘How do the thermal Hall conductivity and Nernst conductivity of the type-I phase differ qualitatively and quantitatively from the type-II phase when the underlying Weyl Hamiltonian supports higher topological charge $n > 1$?’’ This paper is an attempt to answer the above question; in particular, our work yields a general framework for Weyl systems from which the single-Weyl results can be obtained directly.

We find for $n > 1$ ($n = 1$) that the position of the Weyl point can be tuned in a nontrivial (trivial) manner and the Fermi surface gets renormalized with both momentum-dependent and -independent (only momentum-independent) terms. These additional interesting features in the $n > 1$ case heavily influence the subsequent transport properties. The momentum-independent term gives n times the single-Weyl results for a conductivity tensor in its leading order while the dependent terms can lead to subleading correction in the conductivity tensor. Our study further suggests that the vacuum contribution becomes cutoff dependent, unlike the $n = 1$ case, due to the coupling of the $U(1)$ gauge field to the anisotropic dispersion that contains higher momentum modes. In addition to the logarithmic cutoff dependence in the Fermi surface contribution for type-II $n = 1$ WSMs, we find a strong algebraic cutoff dependence for $n \geq 2$. Interestingly, the Fermi surface contribution for type-I mWSMs continues to show a cutoff-independent response, similar to the observation for $n = 1$ mWSMs. Type-I mWSMs behave in a dissimilar manner as compared to type-II mWSMs, as a function of the chemical potential; this is very clearly visible when the Nernst conductivity is investigated. We wish to note that the results presented here pertain to the minimal model and further investigation is needed to verify our claims.

The paper is organized as follows: Sec. II discusses the equilibrium and nonequilibrium low-energy model Hamiltonian and compares it with the single-WSM case. We then study the Berry curvature and anomalous Hall conductivity in detail in Sec. III. Next in Sec. IV, we present our analytical results for optical conductivity using Floquet-Kubo formalism and extensively analyze the vacuum and Fermi surface contribution. In Sec. V we pictorially represent the distinctive behaviors of type-I and type-II mWSMs, and discuss the underlying physics. We present our conclusions in Sec. VI.

II. EFFECTIVE FLOQUET HAMILTONIAN

The low-energy Hamiltonian for a multinode WSM of monopole charge n near each Weyl point is given by [73]

$$H_{\mathbf{k}}^s = \hbar C_s (k_z - sQ) + \hbar \alpha_n \boldsymbol{\sigma} \cdot (\mathbf{n}_{\mathbf{k}} - s\mathbf{e}). \quad (1)$$

The lattice model for mWSMs can be shown to reduce in the above low-energy model [74]. Here, $s = \pm$ indicates the chirality of nodes, $\mathbf{n}_{\mathbf{k}} = [k_{\perp}^n \cos(n\phi_{\mathbf{k}}), k_{\perp}^n \sin(n\phi_{\mathbf{k}}), \frac{vk_z}{\alpha_n}]$, $\mathbf{e} = (0, 0, Q)$, and $2Q$ is the separation between two Weyl nodes. $\boldsymbol{\sigma} = [\sigma_x, \sigma_y, \sigma_z]$ is the vectorized Pauli matrix, and α_n is the mWSM coupling which reduces to the Fermi velocity v when $n = 1$. We define the x - y plane azimuthal angle $\phi_{\mathbf{k}} = \arctan(\frac{k_y}{k_x})$, and the in-plane momentum $k_{\perp} = \sqrt{k_x^2 + k_y^2}$. The Hamiltonian (1) represents the two Weyl nodes $(0, 0, \pm Q)$, located at the same energy and separated by a distance $2Q$, while C_s indicates the tilt parameter associated with the s Weyl node. Type-I mWSMs correspond to $|C_s|/v \ll 1$ while for type-II mWSMs we have $|C_s|/v \gg 1$. We restrict ourselves

to the inversion-symmetric tilt given by $sC_s = C$. We cast the above Hamiltonian in matrix notation:

$$H_{\mathbf{k}}^s = \begin{bmatrix} \hbar C_s(k_z - sQ) + s\hbar v(k_z - sQ) & s\hbar\alpha_n(k_x - ik_y)^n \\ s\hbar\alpha_n(k_x + ik_y)^n & \hbar C_s(k_z - sQ) - s\hbar v(k_z - sQ) \end{bmatrix}. \quad (2)$$

Hereafter, we use natural units and set $\hbar = c = k_B = 1$. We now examine the effect of circularly polarized light on the mWSM. Under the influence of a periodic optical driving with electric field of frequency ω , $\mathbf{E}(t) = E_0(-\cos \omega t, \sin \omega t, 0)$, the Hamiltonian transforms via the Peierls substitution $k_i \rightarrow k_i - A_i$, where the vector potential is given by $\mathbf{A}(t) = \frac{E_0}{\omega}(\sin \omega t, \cos \omega t, 0)$, in the Landau gauge. The gauge-dependent momenta transform as $k_x \rightarrow k'_x = k_x - A_0 \sin \omega t$, $k_y \rightarrow k'_y = k_y - A_0 \cos \omega t$, and $k_z \rightarrow k'_z = k_z$. The driving amplitude of the vector potential is related to the amplitude of the electric field by $A_0 = \frac{E_0}{\omega}$. Considering the fact that $(k'_x \pm ik'_y)^n = \sum_{m=1}^n (k_{\perp} e^{\pm i\phi})^{n-m} (A_0)^m e^{\pm im(\frac{\pi}{2} - \omega t)^n} C_m$, where ${}^n C_m = \frac{n!}{(n-m)!m!}$ represents the combinatorial operator, the time-dependent Hamiltonian takes the form

$$H_{\mathbf{k}}^s(\mathbf{A}, t) = s\sigma_+(k'_x + ik'_y)^n + s\sigma_-(k'_x - ik'_y)^n + C(k_z - sQ) + v(k_z - sQ)\sigma_z. \quad (3)$$

Solving the problem with a time-dependent potential may be out of the reach of analytical tractability. Instead, we resort to using Floquet's theorem and the extracting the subleading order term in the high-frequency Van Vleck expansion, to obtain a closed-form expression for the effective Hamiltonian $H_{\mathbf{k}}^F$. We note that one can numerically solve an extended Floquet Hamiltonian, defined in the Hilbert space $\mathcal{T} \otimes \mathcal{H}$ (with \mathcal{H} being the Hilbert space of static Hamiltonian and \mathcal{T} being the Hilbert space associated with multiphoton dressed states), to obtain the quasistates and quasienergies [75]. From a mathematical point of view, one can also use the Lie algebra technique and a decomposition of the evolution on each group generator to obtain an effective Hamiltonian [76]. However, the Van Vleck expansion is more tractable as the whole Hilbert space of extended Floquet Hamiltonian gets projected onto the zero-photon subspace: $\mathcal{T} \otimes \mathcal{H} \rightarrow \mathcal{T}_0 \otimes \mathcal{H} = \mathcal{H}$. All the eigenvectors of the effective Hamiltonian, obtained from Van Vleck expansion, are the projection of the original eigenvectors onto the model space \mathcal{H} with the true quasienergies. This shows the real usefulness of the Van Vleck expansion where one can get a closed-form expression under the high-frequency approximation.

In this limit, one can describe the dynamics of the driven system over a period T in terms of the effective Floquet Hamiltonian: $H_{\mathbf{k}}^F \approx H_{\mathbf{k}}^s + V_{\mathbf{k}}^s$, where $V_{\mathbf{k}}^s$ represents the perturbative driving term. We restrict ourselves to contributions of order $1/\omega$ throughout the paper, and the form of $V_{\mathbf{k}}^s$ is given by

$$V_{\mathbf{k}}^s = \sum_{p=1}^{\infty} \frac{[V_{-p}, V_p]}{p\omega}, \quad (4)$$

with $V_p = \frac{1}{T} \int_0^T H_{\mathbf{k}}^s(\mathbf{A}, t) e^{ip\omega t} dt$ and $\omega = \frac{2\pi}{T}$. Evaluating $V_{\mathbf{k}}^s$ for our system, we arrive at

$$V_p = s\alpha_n \sum_{m=1}^n (k_{\perp})^{n-m} (-A_0)^m {}^n C_m = \begin{bmatrix} 0 & e^{-i[(n-m)\phi + m\frac{\pi}{2}]} \delta_{p,-m} \\ e^{i[(n-m)\phi + m\frac{\pi}{2}]} \delta_{p,-m} & 0 \end{bmatrix}. \quad (5)$$

Using the result in (5) and evaluating the commutator in (4), we find that the effective Floquet Hamiltonian takes the form

$$H_{\mathbf{k}}^F = H_{\mathbf{k}}^s + V_{\mathbf{k}}^s = C_s(k_z - sQ) + s\alpha_n \boldsymbol{\sigma} \cdot (\mathbf{n}_{\mathbf{k}} - sQ\hat{e}_z) + \frac{\alpha_n^2}{\omega} \sum_{p=1}^n \frac{1}{p} \left({}^n C_p A_0^p \right)^2 k_{\perp}^{2n-2p} \sigma_z = C_s(k_z - sQ) + s\alpha_n (\mathbf{n}'_{\mathbf{k}} - sQ\hat{e}_z) \cdot \boldsymbol{\sigma} \quad (6)$$

with $\mathbf{n}'_{\mathbf{k}} = (k_{\perp}^n \cos(n\phi_k), k_{\perp}^n \sin(n\phi_k), T_{\mathbf{k}}/\alpha_n)$. In all subsequent analysis, we define $T_{\mathbf{k}} \equiv vk_z + \frac{\alpha_n^2}{\omega} \sum_{p=1}^n \beta_p^n k_{\perp}^{2(n-p)} \equiv \Delta_n + T'_{\mathbf{k}}$, with $T'_{\mathbf{k}} \equiv vk_z + \frac{\alpha_n^2}{\omega} \sum_{p=1}^{n-1} \beta_p^n k_{\perp}^{2(n-p)}$, and $\beta_p^n = ({}^n C_p A_0^p)^2/p$. The momentum-independent contribution to the Floquet Hamiltonian acquires the form $\Delta_n = \frac{\alpha_n^2 A_0^{2n}}{n\omega}$. It clear from the construction of (6) that the effective Hamiltonian embodies terms which couple higher momentum modes (modes which diverge faster than k as $k \rightarrow \infty$) of the Weyl fermion to the photon. This can induce a "non-renormalizable" nature to the theory, which as we shall see becomes strongly dependent on a momentum cutoff. This phenomenon is very similar to the theory of quantum electrodynamics with massive operators in high-energy physics. The extra terms, absent for $n = 1$, appear due to the anisotropic energy dispersion of the static mWSM Hamiltonian (1). A close inspection of effective Hamiltonian (6) suggests that circularly polarized light cannot open up a gap in WSMs as the time-reversal symmetry is intrinsically broken in static Hamiltonian (1); instead the position of the Weyl points shifts from $(0, 0, sQ) \rightarrow (0, 0, sQ - \Delta_n)$. We note here $T'_{\mathbf{k}} = vk_z$ for $\mathbf{k} = (0, 0, k_z)$. Interestingly, unlike the single-Weyl case where the shift Q quadratically varies with driving amplitude A_0^2 , the shift in the Weyl point for mWSMs Δ_n is coupled with monopole charge n as $\Delta_n = \frac{\alpha_n^2 A_0^{2n}}{n\omega}$. Therefore, Weyl points receive a topological-charge-dependent shift under irradiation. The terms containing k_{\perp} in $T'_{\mathbf{k}}$ would lead to subleading corrections in transport properties.

The effective quasienergies obtained from the effective Floquet Hamiltonian (6) are thus

$$E_{\mathbf{k}}^F = C_s(k_z - sQ) \pm s\sqrt{\alpha_n^2 k_{\perp}^{2n} + T_{\mathbf{k}}^2}, \quad (7)$$

leading to the established result: $E_{\mathbf{k}}^F(n=1) = C_s(k_z - sQ) \pm s\sqrt{v^2k_{\perp}^2 + (vk_z + \Delta_1)^2}$ as $\alpha_1 = v$. One can observe that the k_{\perp} term in $T_{\mathbf{k}}$ is absent for conical dispersion while for $n > 1$, the distortion anisotropy in conical dispersion leads to terms dependent on k_{\perp} in $T_{\mathbf{k}}$. For completeness, we note that the static energy of an mWSM Hamiltonian with no driving is obtained by diagonalizing the Hamiltonian (1) to obtain $E_{\mathbf{k}}^0 = C_s(k_z - sQ) \pm \sqrt{\alpha_n^2 k_{\perp}^{2n} + v^2 k_z^2}$. Therefore, one can clearly see that the external optical field parameters get coupled with momentum k_{\perp} leading to the complicated form of $T_{\mathbf{k}}$ in Eq. (7). In particular, the nature of the Floquet dispersion (7) changes due to the coupling of the incident light parameter A_0 and ω with the momentum k_{\perp} and the topological charge n . Another interesting feature of the Floquet dispersion is that k_z gets coupled to k_{\perp} , which is not noticed for irradiated single WSMs. Apart from these characteristic changes, the Floquet spectrum remains gapless at $(0, 0, \pm Q - \Delta_n)$. The extensive analysis of the Floquet dispersion can be shown to exhibit a few distinct behaviors as compared to static dispersion [74].

III. BERRY CURVATURE

It is very important to study geometric phases in any topological system as the anomalous response function is directly given by the Berry curvature. Here our aim would be to investigate the effect of the driving on the Berry curvature and subsequently on the anomalous transport. Before going into detail, we begin by defining the Berry curvature associated with the Floquet Hamiltonian $H_{\mathbf{k}}^F$. The Berry curvature of the m th band for a Bloch Hamiltonian $H(k)$, defined as the Berry phase per unit area in the k space, is given by [77]

$$\Omega_a^m(\mathbf{k}) = (-1)^m \frac{1}{4|n_{\mathbf{k}}|^3} \epsilon_{abc} n_{\mathbf{k}} \cdot \left(\frac{\partial \mathbf{n}_{\mathbf{k}}}{\partial k_b} \times \frac{\partial \mathbf{n}_{\mathbf{k}}}{\partial k_c} \right). \quad (8)$$

The explicit form of the Berry curvature associated with the Weyl node having chirality s as obtained from Floquet effective Hamiltonian (6) is given by

$$\Omega_F^{\pm,s}(\mathbf{k}) = \pm \frac{1}{2} \frac{1}{|E_{\mathbf{k}}^F|^3} (nv\alpha_n^2 k_{\perp}^{2n-1} \cos \phi_{\mathbf{k}}, nv\alpha_n^2 k_{\perp}^{2n-1} \sin \phi_{\mathbf{k}}, -n\beta_{\mathbf{k}} \alpha_n^2 k_{\perp}^{2n} + T_{\mathbf{k}} n^2 \alpha_n^2 k_{\perp}^{2n-2}), \quad (9)$$

with $\beta_{\mathbf{k}} = \frac{\alpha_n^2}{\omega} \sum_{p=1}^n (2n-2p) \beta_p^n k_{\perp}^{2n-2p-2}$. We note that the $+$ ($-$) sign refers to the valence (conduction) band and chirality $s = \pm 1$. The Berry curvature remains unaltered irrespective of the chirality of the Weyl nodes, i.e., $\Omega^{\pm,+} = \Omega^{\pm,-}$. This is due to the fact that the chirality factor s appears in the Hamiltonian with all σ_i 's; a close inspection suggests that s gets canceled from the numerator and denominator in Eq. (8).

One can obtain regular static Berry curvature when $A_0 = 0$, $\beta_{\mathbf{k}} = 0$, and $T_{\mathbf{k}} = vk_z$. The static Berry curvature using Hamiltonian (1) becomes

$$\Omega_0^{\pm,s}(\mathbf{k}) = \pm \frac{1}{2} \frac{1}{|E_{\mathbf{k}}^0|^3} (nv\alpha_n^2 k_{\perp}^{2n-1} \cos \phi_{\mathbf{k}}, nv\alpha_n^2 k_{\perp}^{2n-1} \sin \phi_{\mathbf{k}}, \times n^2 v \alpha_n^2 k_{\perp}^{2n-2} k_z). \quad (10)$$

Therefore, one can observe that $\Omega_z(\mathbf{k})$ is modified due to the driving, while the remaining two components of $\Omega_F^{\pm}(\mathbf{k})$ receive the correction from the effective energy $E_{\mathbf{k}}^F$ appearing in the denominator. This suggests that anomalous conductivity σ_{xy}^a would be heavily modified due to the driving as compared to σ_{xz}^a and σ_{yz}^a . We shall analyze this extensively in what follows.

Now, turning to the $n=1$ case, the Berry curvature for the driven single-WSM case is given by $\Omega_F^{\pm,s}(\mathbf{k}, n=1) = (k_x, k_y, k_z + v^3 \Delta_1) / |E_{\mathbf{k}}^0(n=1)|^3$. One can clearly observe that for driven mWSMs all components of $\Omega(\mathbf{k})$ depend on k_{\perp} , while for the driven single-WSM case individual components are composed of separate momentum. Thus the dispersion anisotropy of the $n > 1$ mWSMs imprints effects which are absent for the single-WSM case. Importantly, even for $\Omega_z(\mathbf{k})$ in single WSMs, the momentum-independent term $\Delta_1 \sim A_0^2$ bears the signature of periodic driving. For $n > 1$, the topological charge gets coupled with the driving parameter which leads to a more complex form of $\Omega_z(\mathbf{k})$ as compared to the $n=1$ case.

We shall compute the anomalous Hall conductivity $\sigma_{F,xy}^a$, considering the effective Floquet Hamiltonian, from the z component of Berry curvature in Eq. (10). In order to obtain a closed-form result in the leading order, we neglect $\beta_{\mathbf{k}}$ as $\omega \rightarrow \infty$ as the effective energy in the denominator bears the correction terms due to driving as shown in Eq. (7). On the other hand, we consider the effect of the Floquet driving on the cutoff limit of k_z integration. In particular, $z_l = -\Lambda - sQ \rightarrow z'_l$ and $z_u = \Lambda - sQ \rightarrow z'_u$ with $z'_l = -\Lambda - sQ + s\Delta_n$ and $z'_u = \Lambda - sQ + s\Delta_n$. Therefore, one can safely consider the static energy in the denominator, and we shall motivate this assumption extensively while discussing the vacuum contribution Sec. IV A. The anomalous contribution to leading order is thus given by

$$\begin{aligned} \sigma_{F,xy}^a &= e^2 \int \frac{d\mathbf{k}}{4\pi^2} \sum_s \Omega_F^{-s}(\mathbf{k}) \\ &\simeq -\frac{ne^2}{4\pi^2} \int_{z'_l}^{z'_u} \int_0^{\infty} dk_{\perp} dk_z \frac{k_z k_{\perp}}{(k_z^2 + k_{\perp}^2)^{3/2}} \\ &\simeq -\frac{ne^2}{2\pi^2} (Q + \Delta_n). \end{aligned} \quad (11)$$

We have considered cylindrical polar coordinates for the convenience of the integration along with the following rescaling: $k_z \rightarrow k_z/v$ and $k_{\perp} \rightarrow k_{\perp}^{1/n} \alpha_n^{-1/n}$. It is noteworthy that this anomalous Hall coefficient has a topological property due to the appearance of the monopole charge. For the static system, it is just given by $-\frac{ne^2}{2\pi^2} Q$. Since the Berry curvature of the filled valence band remains the same for both the nodes with opposite chiralities, the result obtained considering these two nodes is just double that obtained in the single node.

We now connect our findings to the transport phenomena in the mWSMs. It has been shown that there exist n Fermi arcs for a mWSM with topological charge n [25], and we know the transport is mainly governed by the surface states present in the Fermi arc for WSMs. Interestingly, driving shifts the position of Weyl points $\pm Q \rightarrow \pm Q + \Delta_n$; this leads to the modification in Fermi arc for the irradiated case as compared to the static case. As a result, transport properties

receive additional corrections from driving. It has been shown that the Fermi arc can be tuned using the Floquet replica technique when a WSM is irradiated with circularly polarized light [78]. The factor n in front of Eq. (11) signifies that the effective Floquet Hamiltonian still supports n Fermi arcs. We here mention that the neglected β_k term would give rise to subleading nontopological contributions. Since we wish to probe the question of transport due to laser driving, it would be appropriate to investigate the optical conductivity using Floquet-Kubo formalism. However, we note at the outset that one can find an expression similar to that given in Eq. (11) while calculating the vacuum contribution of optical conductivity up to leading order.

IV. CONDUCTIVITY TENSOR

Having derived the Berry-curvature-induced anomalous Hall conductivity, we shall now systematically formulate the conductivity tensor using the current-current correlation function. This is constructed using the Matsubara Green's function method. The current-current correlation is written as

$$\begin{aligned} \prod_{\mu\nu}(\Omega, \mathbf{k}) = T \sum_{\omega_n} \sum_{s=\pm} \int \frac{d^3k}{(2\pi)^3} J_\mu^{(s)} G_s(i\omega_n, \mathbf{k}) \\ \times J_\nu^{(s)} G_s(i\omega_n - i\Omega_m, \mathbf{k} - \mathbf{q})|_{i\Omega_m \rightarrow \Omega + i\delta}. \end{aligned} \quad (12)$$

Here, $\mu, \nu = \{x, y, z\}$, T is the temperature, ω_n and Ω_n are the fermionic and bosonic Matsubara frequencies, and G is the single-particle Green's function. The Hall conductivity can now be derived from the zero frequency $\Omega \rightarrow 0$ and zero-wave-vector limit.

Using the current-current correlation (12), one can define the static conductivity tensor σ_{ab}^0 . We here use the form of the time-averaged conductivity tensor σ_{ab}^F in the form of the Kubo formula, modified for the Floquet states as

$$\begin{aligned} \sigma_{ab}^F = i \int \frac{d^3\mathbf{k}}{(2\pi)^3} \sum_{\alpha \neq \beta} \frac{f_\beta(\mathbf{k}) - f_\alpha(\mathbf{k})}{\epsilon_\beta(\mathbf{k}) - \epsilon_\alpha(\mathbf{k})} \\ \times \frac{\langle \Phi_\alpha(\mathbf{k}) | J_b | \Phi_\beta(\mathbf{k}) \rangle \langle \Phi_\beta(\mathbf{k}) | J_a | \Phi_\alpha(\mathbf{k}) \rangle}{\epsilon_\beta(\mathbf{k}) - \epsilon_\alpha(\mathbf{k}) + i\eta}, \end{aligned} \quad (13)$$

which resembles the standard form of the Kubo formula where $J_{a(b)}$ represents the current operator, the $|\Phi_\alpha(\mathbf{k})\rangle$ represents the states of the effective Floquet Hamiltonian (6), and ϵ_α represent the corresponding quasienergies. The f_α represent the occupations which in general could be nonuniversal in systems which are out of equilibrium. In such cases, the steady-state occupations can take the form of a Fermi-Dirac distribution associated with the quasienergies of the Floquet states, depending on the characteristics of the drive. The Matsubara formalism turns out to hold for Floquet states as well [30]. The method of Floquet Kubo formalism has been widely used in calculating optical Hall conductivity in open and closed quantum systems [79].

One can start from Luttinger's phenomenological transport equations [80] for the electric and energy DC currents. The energy current originates from the combination of heat current J_Q and energy transported by the electric current J_E in the presence of electromagnetic field while the underlying system is characterized by a finite chemical potential μ and temper-

ature T . Within the Fermi liquid limit $k_B T \ll |\mu|$, the Mott rule and the Wiedemann-Franz law relate the thermopower α and thermal conductivity K , respectively, to the electric conductivity σ [81–83]:

$$\alpha_{ab} = eLT \frac{d\sigma_{ab}}{d\mu}, \quad K_{ab} = LT\sigma_{ab}. \quad (14)$$

Here, α_{ab} is the Nernst conductivity, K_{ab} is the thermal Hall conductivity, and $L = \pi^2 k_B^2 / 3e^2$ is the Lorentz number. These formulas are assumed to be valid for the effective time-independent Floquet Hamiltonian setup [30], and we shall investigate them in what follows.

One can define the current operator from the effective Floquet Hamiltonian $H_{\mathbf{k}}^F$ [Eq. (6)]:

$$J_\mu = e \frac{\partial H_{\mathbf{k}}^F}{\partial k_\mu}. \quad (15)$$

In order to derive J_μ , we consider the leading order term neglecting the $\partial T_{\mathbf{k}} / \partial k_\mu$ term as it contains the $1/\omega$ factor. We note that the current operator obtained in this manner would be the same as the static current operator for the mWSM Hamiltonian. This leading order term can be further confirmed by the zeroth-order Fourier component of the current operator as shown in the Supplemental Material [74]. However, one can indeed consider the full current operator with $\partial T_{\mathbf{k}} / \partial k_\mu$ to obtain the higher-order corrections. The effect of the $T_{\mathbf{k}}$ term is also encoded in the single-particle Green's function G_s . We compute the optical conductivity by using the complete expression of G and approximated current operator.

In terms of σ 's, we can write up to leading order as

$$J_x \approx esn\alpha_n k_\perp^{n-1} \{ \cos[(n-1)\phi_{\mathbf{k}}] \sigma_x + \sin[(n-1)\phi_{\mathbf{k}}] \sigma_y \}, \quad (16)$$

$$J_y \approx esn\alpha_n k_\perp^{n-1} \{ \cos[(n-1)\phi_{\mathbf{k}}] \sigma_y - \sin[(n-1)\phi_{\mathbf{k}}] \sigma_x \}. \quad (17)$$

The point to note here is that J_x and J_y both depend on k_x and k_y , which is in contrast to the single-WSM case where $J_i \sim k_i \sigma_i$. The anisotropic nature of dispersion of the mWSM Hamiltonian thus engraves its effect on the current operator.

Employing the current-current correlation and performing a detailed calculation [74], we arrive at the conductivity tensor as

$$\begin{aligned} \sigma_{xy} = \frac{e^2 n^2 \alpha_n^2}{4\pi^2} \sum_{s=\pm} \int_0^\infty dk_\perp k_\perp^{2n-1} \int_{-\Lambda}^\Lambda dk_z \\ \times \frac{sv(k_z - Q) + \frac{sv^2}{\omega} \sum_{p=1}^n \beta_p k_\perp^{2(n-p)}}{\left\{ \left[\frac{sv^2}{\omega} \sum_{p=1}^n \beta_p k_\perp^{2(n-p)} + sv(k_z - sQ) \right]^2 + \alpha_n^2 k_\perp^{2n} \right\}^{3/2}} \\ \times [n_F(E_{\mathbf{k}}^{F,-}) - n_F(E_{\mathbf{k}}^{F,+})], \end{aligned} \quad (18)$$

where Λ is the ultraviolet cutoff of the k_z integral, $n_F(E) = \frac{1}{e^{\beta(E-\mu)} + 1}$ is the Fermi-Dirac distribution function, and $\beta = 1/T$ is the inverse temperature. The total optical conductivity (18) is the sum of vacuum and Fermi surface contributions that we shall extensively calculate below. We note that due to the existence of external and internal energy scale ω and μ , the cutoff Λ plays an important role in achieving physically

meaningful results. This cutoff is ultraviolet in nature and can in principle depend on the details of the material.

A. Vacuum contribution

In this section, we investigate the vacuum contribution which is obtained in the limit $[n_F(E_{\mathbf{k}}^{F,-}) - n_F(E_{\mathbf{k}}^{F,+})] \rightarrow 1$. Physically this means that the valence (conduction) band is completely filled (empty). This vacuum contribution amounts to an intrinsic contribution that remains finite for $\mu \rightarrow 0$. Computationally, this refers to the situation where the upper limit k_{\perp} is considered to be ∞ in the literature. With suitable redefinitions and linear integration variable shifts, we arrive at

$$\sigma_{xy}^{vac} = \frac{e^2 n^2 \alpha_n^2}{4\pi^2} \sum_{s=\pm} \int_0^{\infty} dk_{\perp} k_{\perp}^{2n-1} \int_{-\Lambda-sQ+\frac{s\omega}{\omega} A_0^{2n}}^{\Lambda-sQ+\frac{s\omega}{\omega} A_0^{2n}} \times \frac{[svk_z + \frac{\alpha_n^2}{\omega} \sum_{p=1}^{n-1} \beta_p^n k_{\perp}^{2(n-p)}]}{[(\frac{\alpha_n^2}{\omega} \sum_{q=1}^{n-1} \beta_q^n k_{\perp}^{2(n-q)})^2 + \alpha_n^2 k_{\perp}^{2n}]^{3/2}}. \quad (19)$$

We will compute the vacuum contribution using two separate procedures involving suitable approximations and then compare the results obtained.

1. Coordinate transformation method

The method prescribed in this section relies on the fact that while several quantities are set to infinity in a computation, in order to get physically plausible answers one might need to define the order in which the limits are taken. For computation of the integrals, the following coordinate map $\mathcal{M} : \mathbb{R}^2 \rightarrow \mathbb{R}^2$ is prescribed with the action $k_{\perp} \rightarrow k'_{\perp} = k_{\perp}^{\frac{1}{n}} \alpha_n^{-\frac{1}{n}}$ and $k_z \rightarrow k_z$. With this coordinate transformation, the vacuum contribution of the conductivity tensor looks like

$$\sigma_{xy}^{vac} = -\frac{e^2 n \alpha_n^{2-\frac{2}{n}}}{4\pi^2} \sum_{s=\pm} s \int_{z_l}^{z_u} \int_{x_l}^{x_u} \frac{k_{\perp} T_{\mathbf{k}}}{(k_{\perp}^2 + T_{\mathbf{k}}^2)^{3/2}} dk_{\perp} dk_z. \quad (20)$$

Here, the upper and lower limits of the integrals have been determined with appropriate physical justifications [74]:

$$x_l = 0, \quad x_u = \Lambda_{\perp}, \quad (21)$$

$$z_u = v(\Lambda - sQ) + s \left(\Delta_n + \frac{\alpha_n^2}{\omega} \sum_{p=1}^{n-1} \beta_p^n \alpha_n^{\frac{2(p-n)}{n}} \Lambda_{\perp}^{\frac{2(n-p)}{n}} \right),$$

$$z_l = v(-\Lambda - sQ) + s \left(\Delta_n + \frac{\alpha_n^2}{\omega} \sum_{p=1}^{n-1} \beta_p^n \alpha_n^{\frac{2(p-n)}{n}} \Lambda_{\perp}^{\frac{2(n-p)}{n}} \right).$$

Λ_{\perp} is the cutoff for the k_{\perp} integral. One can segregate $z_{l,u}$ from Λ_{\perp} : $z_{l,u} = z'_{l,u} + s \frac{\alpha_n^2}{\omega} X_{\Lambda_{\perp}}$ with $X_{\Lambda_{\perp}} = \sum_{p=1}^{n-1} \beta_p^n \alpha_n^{\frac{2(p-n)}{n}} \Lambda_{\perp}^{\frac{2(n-p)}{n}}$ and $z'_{l,u} = v(\mp \Lambda - sQ) + s \Delta_n$. Hence one has to handle this cutoff with care, and the issue reduces to the order of taking limits. We again stress that the high-frequency Floquet effective Hamiltonian is valid when ω is larger than the bandwidth not permitting any real electronic transitions. Keeping this in mind, the subleading $1/\omega$ order correction that we want to extract is preserved as we execute

the k_{\perp} integral followed by the k_z integral. We note that while solving the k_{\perp} integral, without loss of generality Λ_{\perp} is considered to be large as compared to Λ . Importantly, Λ_{\perp}/ω is small compared to Λ and hence $X_{\Lambda_{\perp}}$ is a subleading term since ω sets the dominant energy scale in the problem. Taken collectively, the subleading $X_{\Lambda_{\perp}}$ term is held finite during the k_{\perp} integration and this leads to the Λ_{\perp} dependence reappearing through the limits of the k_z integral. In a nutshell, our result is applicable when $\omega \gg \Lambda_{\perp} \gg \Lambda$. We justify the above assumptions for the high-frequency Floquet effective Hamiltonian $H_{\mathbf{k}}^F$ (6) that is derived from a low-energy minimal model (1).

Finally, we obtain the vacuum contribution of conductivity in mWSMs,

$$\sigma_{xy}^{vac} = n \frac{e^2 Q \alpha_n^{2-\frac{2}{n}}}{2\pi^2} - n \frac{e^2 \alpha_n^{2-\frac{2}{n}}}{2\pi^2} \left[\Delta_n - \frac{\alpha_n^2}{\omega v} \sum_{p=1}^{n-1} \beta_p^n \Lambda_{\perp}^{2(n-p)} \right]. \quad (22)$$

Here, Δ_n and β_p^n are the contributions appearing as an effect of light. For mWSMs, the light-induced Weyl node position depends on the topological charge associated with the Weyl node. This shift in Weyl nodes reduces to a driving-parameter-dependent constant value as observed in the irradiated single WSMs. One can easily recover the $n = 1$ behavior of the gap where Δ_1 varies quadratically with the amplitude of driving A_0 [30]. For $n > 1$ further corrections, due to higher-order curvature of the Floquet Hamiltonian, contribute in terms of the cutoff of the low-energy model.

2. Series expansion method

We shall now proceed with a physically justified alternative method to compute Λ_{\perp} in terms of the k_z cutoff. The idea here is to expand the denominator around its unperturbed static energy in increasing powers of driving period $1/\omega \rightarrow 0$ as $\omega \rightarrow \infty$. The perturbative expansion is then given by

$$k_{\perp}^2 + T_{\mathbf{k}}^2 \approx E_{\mathbf{k}}^2 + \frac{2vk_z \alpha_n^2}{\omega} \sum_{p=1}^{n-1} \beta_p^n \alpha_n^{\frac{2(p-n)}{n}} k_{\perp}^{\frac{2(n-p)}{n}}. \quad (23)$$

One can then note that for $n = 2$, only β_1^n exists while for $n = 3$, β_1^n and β_2^n both exist. $E_{\mathbf{k}} = \sqrt{k_{\perp}^2 + v^2 k_z^2}$ is the bare static energy of the single WSM in the absence of tilt. Considering $X_{k_{\perp}} = \sum_{p=1}^{n-1} \beta_p^n \alpha_n^{\frac{2(p-n)}{n}} k_{\perp}^{\frac{2(n-p)}{n}}$, we now express the integrand as

$$\frac{T_{\mathbf{k}}}{(k_{\perp}^2 + T_{\mathbf{k}}^2)^{3/2}} \approx \frac{1}{E_{\mathbf{k}}^3} \left[vk_z - \frac{3v^2 k_z^2 \alpha_n^2}{E_{\mathbf{k}}^2 \omega} X_{k_{\perp}} + \frac{\alpha_n^2}{\omega} X_{k_{\perp}} \left(1 - \frac{3vk_z \alpha_n^2}{E_{\mathbf{k}}^2 \omega} X_{k_{\perp}} \right) \right]. \quad (24)$$

We explicitly write σ_{xy}^{vac} for $n = 2$ (neglecting the $1/\omega^2$ term) as

$$\sigma_{xy}^{vac}(n=2) = -\frac{e^2 n \alpha_n^{2-\frac{2}{n}}}{4\pi^2} \sum_{s=\pm} s \int_{z'_l}^{z'_u} \int_0^{\infty} \frac{k_{\perp} T_{\mathbf{k}}}{(k_{\perp}^2 + T_{\mathbf{k}}^2)^{3/2}} dk_{\perp} dk_z$$

$$\begin{aligned} &\approx -\frac{e^2 n \alpha_n^{2-\frac{2}{n}}}{4\pi^2} \sum_{s=\pm} s [v(z_l + z_u) + v^2 \alpha_n \beta_1^n (z'_l - z'_u)] \\ &\approx -\frac{e^2 n \alpha_n^{2-\frac{2}{n}}}{4\pi^2} \left[v(-2Q + 2\Delta_n) + \frac{2v^2 \alpha_n \beta_1^n}{\omega} \Lambda \right]. \end{aligned} \quad (25)$$

In this derivation, we ignore the divergent contributions coming from the integrals having higher powers of k_\perp in the numerator. These types of terms, being artifacts of the underlying low-energy model, do not appear in the lattice model. In order to obtain Λ_\perp , we equate the coefficient of $1/\omega$ from Eq. (25) and Eq. (22). We find that Λ_\perp linearly depends on Λ' : $\Lambda_\perp = 2v^2 \Lambda'$. For $n = 3$, we find

$$\begin{aligned} \sigma_{xy}^{vac}(n=3) = &-\frac{e^2 n \alpha_n^{2-\frac{2}{n}}}{4\pi^2} \left\{ v(-2Q + 2\Delta_n) \right. \\ &- \frac{2v^2 \alpha_n^{\frac{2}{n}} \beta_1^n}{\omega \sqrt{\pi}} \Gamma\left(\frac{5}{6}\right) \Gamma\left(\frac{5}{3}\right) \left(\frac{|z_l|^{\frac{4}{n}} + z_u^{\frac{4}{n}}}{4/3}\right) \\ &+ \frac{\beta_2^n}{\omega} \left[-\frac{3v^2 \alpha_n^{\frac{4}{n}}}{2\sqrt{\pi}} \Gamma\left(\frac{7}{6}\right) \Gamma\left(\frac{7}{3}\right) \left(\frac{|z_l|^{\frac{2}{n}} + z_u^{\frac{2}{n}}}{2/3}\right) \right. \\ &\left. \left. + \frac{\alpha_n^{\frac{4}{n}}}{\sqrt{\pi}} \Gamma\left(\frac{1}{6}\right) \Gamma\left(\frac{4}{3}\right) \left(\frac{|z_l|^{\frac{2}{n}} + z_u^{\frac{2}{n}}}{2/3}\right) \right] \right\}. \end{aligned} \quad (26)$$

It is noted that contrary to the $n = 2$ case, Λ_\perp is nonlinearly related to Λ' for $n = 3$: $\Lambda_\perp^{\frac{4}{n}} = \eta_1 (|z_l|^{\frac{4}{n}} + z_u^{\frac{4}{n}})$ and $\Lambda_\perp^{\frac{2}{n}} = \eta_2 (|z_l|^{\frac{2}{n}} + z_u^{\frac{2}{n}})$, where $\eta_{1,2}$ can be obtained by matching the coefficient of β_1^n/ω and β_2^n/ω . The relationships between Λ and Λ_\perp derived here are consistency conditions for the model parameters.

B. Fermi surface contribution

We take note of the point that for the calculation of the Fermi surface contribution, one has to consider the finite upper limit in the k_\perp integral as b , a parameter which we compute below. The Fermi surface contribution for a given n becomes

$$\begin{aligned} \sigma_{xy}^{FS}(n) = &n \alpha_n^{2-2/n} \sum_s \int_{z'_l}^{z'_u} dk_z \int_0^b \frac{k_\perp T_{\mathbf{k}}}{(k_\perp^2 + T_{\mathbf{k}}^2)^{3/2}} dk_\perp \\ &\times [\Theta(v^2 k_z^2 + (Ck_z + sC\Delta_n - \mu)^2) - 1]. \end{aligned} \quad (27)$$

In the equation above, $\Theta(x)$ represents the Heaviside function which arises from the zero-temperature Fermi-Dirac distribution. It is then more convenient to write $T_{\mathbf{k}}$ explicitly for $n = 2$ as $T_{\mathbf{k}} = vk_z + \beta_1^n \alpha_n^{-2/n} k_\perp^{2/n}$ and for $n = 3$ as $T_{\mathbf{k}} = vk_z + \beta_1^n \alpha_n^{-4/n} k_\perp^{4/n} + \beta_2^n \alpha_n^{-2/n} k_\perp^{2/n}$. In a more compact notation, for $n = 3$, we define $\beta'_2 = \beta_2^n \alpha_n^{-2/n}$ and $\beta'_3 = \beta_1^n \alpha_n^{-4/n}$, and for $n = 2$, we define $\beta'_2 = \beta_1^n \alpha_n^{-2/n}$ and $\beta'_3 = 0$. On the other hand, $b = \{Ck_z + sC\beta_1 - \mu\}^2 - v^2 k_z^2\}^{1/2}$. Below we shall express all our findings in terms of β'_2 and β'_3 for a general n .

In the leading order approximation, $\beta_1 = O(\frac{1}{\omega})$, $k_z \rightarrow 0$ and μ is held finite. We shall consider the type-I and type-II cases separately: $|C| \gg v$, $b = \mu - Ck_z$ and $|C| \ll v$, $b = (\mu^2 - v^2 k_z^2)^{1/2}$. We again resort to the leading order method

where we permit the $O(1/\omega)$ order term and obtain the following:

$$\sigma_{xy}(n) = \frac{n \alpha_n^{2-2/n}}{v} \int_{z'_l}^{z'_u} dk_z \int_0^b dk_\perp k_\perp (F_{\mathbf{k},1} + F_{\mathbf{k},2} + F_{\mathbf{k},3}) \quad (28)$$

with $F_{\mathbf{k},1} = \frac{k_z}{E_{\mathbf{k}}^3}$, $F_{\mathbf{k},2} = \frac{\beta'_2 k_\perp^{\frac{2}{n}} + \beta'_3 k_\perp^{\frac{4}{n}}}{E_{\mathbf{k}}^3}$, $F_{\mathbf{k},3} = -\frac{3k_z^2 F_{\mathbf{k},2}}{E_{\mathbf{k}}^5}$. We note that in Eq. (28) the leading order term $F_{\mathbf{k},1}$ is also present for the $n = 1$ Weyl node case. Similarly to the vacuum contribution of optical conductivity, the multi-Weyl nature appears here through a multiplicative factor $n \alpha_n^{2-2/n}$. The additional anisotropic and band-bending corrections appear in terms of $1/\omega$ in $F_{\mathbf{k},2}$ and $F_{\mathbf{k},3}$. To obtain a minimal expression, the above derivation is simplified by neglecting the term $F_{\mathbf{k},3}$ as $k_z^2/E_{\mathbf{k}}^3 \rightarrow 0$ for $k_z \rightarrow 0$ considered for the low-energy model. A close inspection suggests that $F_{\mathbf{k},3}$ contains $O(k_\perp^p/\omega^{p'})$ and $O(k_z^q/\omega^{q'})$ with p, q (p', q') < 1 (> 1). As a result, for $\omega \rightarrow \infty$, $F_{\mathbf{k},3}$ can be neglected compared to the leading order terms $F_{\mathbf{k},1}$.

For type-I mWSM, one can keep in mind the fact that b remains always positive. The total contribution from the Fermi surface is given by

$$\begin{aligned} \sigma_{xy}^{FS(I)} \approx &-\frac{e^2 n \alpha_n^{2-2/n}}{4\pi^2} \left\{ (\mu - C\Delta_n) \left[\frac{v}{C^2} \ln\left(\frac{v+C}{v-C}\right) - 2 \right] \right. \\ &+ \beta'_2 a(M) \left[\mu^{\frac{2M}{n}-3} \frac{2v(\mu - C\Delta_n)}{v^2 - C^2} \right. \\ &- \left. \left. \left(\frac{2M}{n} - 3 \right) v^2 \mu^{\frac{2M}{n}-5} \left(\frac{\mu - C\Delta_n}{v^2 - C^2} \right)^3 (3C^2 + v^2) \right] \right. \\ &\left. + \beta'_3 \{M \rightarrow 2M\} \right\} \end{aligned} \quad (29)$$

with

$$a(M) = \frac{\Gamma(\frac{M}{n} + 2)}{(\frac{2M}{n} + 2)(\frac{2M}{n} - 3)\Gamma(\frac{M}{n} + 1)}, \quad (30)$$

with $M = 1$. Therefore, the leading contribution is not just given by $n \alpha_n^{2-2/n}$ multiplied by the $n = 1$ contribution. In this first term μ gets renormalized by $\mu - C\Delta_n$ while Δ_n depends on topological charge n . The other subleading order terms are of order $1/\omega$. The multi-Weyl nature thus imprints its effect on the Fermi surface part of the optical conductivity. We can write a closed-form expression for $v \gg |C|$ as follows,

$$\begin{aligned} \sigma_{xy}^{FS(I)} = &n \frac{\alpha_n^{2-2/n}}{v} \frac{e^2}{4\pi^2} \left[\frac{C(\mu - C\Delta_n)}{6v^2} \right. \\ &+ 4\beta'_2 a(M) \left(\frac{(2\mu)^{2/n-2}}{v} + \frac{(2/n-3)\mu^{2/n-2}}{v} \right) \\ &\left. + 4\beta'_3 a(2M) \left(\frac{2\mu^{4/n-2}}{v} + \frac{(4/n-3)\mu^{4/n-2}}{v} \right) \right]. \end{aligned} \quad (31)$$

Therefore, the total conductivity of a type-I mWSM for a given n is expressed as

$$\alpha_{xy}^I(n) = n \frac{e^2}{4\pi^2} \frac{\alpha_n^{2-2/n}}{v} \left[(Q + \Delta_n) + C \left(\frac{\mu - C\Delta_n}{6v^2} \right) + 4\beta_2'' a(M) \mu^{2/n-2} + 4\beta_3'' a(2M) \mu^{4/n-2} \right], \quad (32)$$

with $\beta_2'' = \beta_2'(\frac{2}{v} + \frac{2/n-3}{v})$ and $\beta_3'' = \beta_3'(\frac{2}{v} + \frac{4/n-3}{v})$. This helps us to write the anomalous thermal Hall conductivity K_{xy}^I and Nernst conductivity α_{xy}^I respectively for the type-I mWSMs as

$$\begin{aligned} K_{xy}^I(n) &= \frac{\pi^2}{3e^2} k_B^2 T \sigma_{xy}^I \\ &= n \frac{T k_B^2}{12} \frac{\alpha_n^{2-2/n}}{v} \left[(Q + \Delta_n) - C \left(\frac{\mu - C\Delta_n}{6v^2} \right) + 4\beta_2'' a(M) \mu^{2/n-2} + 4\beta_3'' a(2M) \mu^{4/n-2} \right]. \end{aligned} \quad (33)$$

One can find

$$\begin{aligned} \alpha_{xy}^I(n) &= \frac{\pi^2}{3e^2} k_B^2 T \frac{d\sigma_{xy}^I}{d\mu} \\ &= n \frac{e k_B^2}{12} \frac{\alpha_n^{2-2/n}}{v} \left[-\frac{C}{6v^2} + 4\beta_2'' a(M) \left(\frac{2}{n} - 2 \right) \times \mu^{2/n-3} + 4\beta_3'' a(2M) \left(\frac{4}{n} - 2 \right) \mu^{4/n-3} \right]. \end{aligned} \quad (34)$$

One can now easily derive the expressions for σ_{xy}^I , K_{xy}^I , and α_{xy}^I for $n = 2$ by considering $\beta_3' = 0$. Comments on the new results for $n = 2$ and $n = 3$ and their characteristic dissimilarities from the $n = 1$ case are now in order. In general, the nonlinear μ dependence comes from the order $1/\omega$ term in the $n > 1$ multi-Weyl case while the linear μ dependence term only appear for $n = 1$.

Let us now explore the thermal responses for the type-II case of mWSMs where the sign of the k_\perp momentum cutoff b depends on k_z . Handling of the k_\perp integral requires extra care as $\text{sgn}(b)$ becomes $+$ ($-$), depending on k_z being $-$ ($+$). $|C| \gg v$ refers to the fact that $v^2 k_z^2 - (Ck_z + sC\Delta_n - \mu)^2 < 0$. Keeping in mind the k_\perp integral, we find

$$\begin{aligned} \sigma_{xy}^{II}(n) &= n \frac{e^2}{4\pi^2} \frac{\alpha_n^{2-2/n}}{v} \left\{ (\Delta_n + Q) \left(-1 + \frac{v}{C} \right) - \frac{v(C\Delta_n - \mu)}{C^2} \ln \left(\frac{C^2 \Lambda}{v(C\Delta_n - \mu)} \right) + \beta_2' a(M) \right. \\ &\times \left[\mu^{\frac{2M}{n}-3} \left(\frac{2\Delta_n v}{C} - 2Q \right) + \left(\frac{2M}{n} - 3 \right) \frac{C \mu^{\frac{2M}{n}-4}}{2} \right. \\ &\left. \left. \times \left(\frac{4\Delta_n^2 v}{C} - 2\Lambda^2 - 2Q^2 \right) \right] + \beta_3' \{M \rightarrow 2M\} \right\} \end{aligned} \quad (35)$$

with $M = 1$. The remarkable point to note here is that the momentum cutoff Λ shows up algebraically in the Fermi surface contribution. However, this is accompanied with the subleading term $O(1/\omega)$. This is indeed a new feature for the anisotropic character of the dispersion in type-II mWSMs. In

type-II single WSMs, the momentum cutoff can only appear logarithmically.

Using the results obtained above, we write the anomalous thermal Hall conductivity for type-II mWSMs:

$$\begin{aligned} K_{xy}^{II}(n) &= nT \frac{k_B^2}{12} \alpha_n^{2-2/n} \left\{ (\Delta_n + Q) \left(\frac{v}{C} - 1 \right) - \frac{v}{C^2} (C\Delta_n - \mu) \ln \left(\frac{C^2 \Lambda}{v(C\Delta_n - \mu)} \right) + \beta_2' a(M) \right. \\ &\times \left[\mu^{2M/n-3} a_2(M) + \mu^{2M/n-4} a_3(M) \right. \\ &\left. \left. + \beta_3' \{M \rightarrow 2M\} \right\} \end{aligned} \quad (36)$$

with $a_2(M) = (2\Delta_n v/C - 2Q)$, $a_3(M) = C(2M/n - 3)(4\Delta_n^2 v/C - 2\Lambda^2 - 2Q^2)$, and $M = 1$. On the other hand, the Nernst conductivity is given by

$$\begin{aligned} \alpha_{xy}^{II}(n) &= ne \frac{k_B^2 \alpha_n^{2-2/n}}{12} \left\{ \frac{1}{C^2} \left[-1 + \ln \left(\frac{C^2 \Lambda}{v(C\Delta_n - \mu)} \right) \right] + \beta_2' a(M) \left[\left(\frac{2M}{n} - 3 \right) \mu^{2M/n-4} a_2(M) \right. \right. \\ &\left. \left. + \left(\frac{2M}{n} - 4 \right) \mu^{2M/n-5} a_3(M) \right] + \beta_3' \{M \rightarrow 2M\} \right\}. \end{aligned} \quad (37)$$

One can easily obtain the $n = 2$ results by considering $\beta_3' = 0$.

V. DISCUSSION OF RESULTS

We now discuss some important aspects of our findings on the distinguishing transport features of type-I and type-II mWSMs. First of all, we emphasize the significant results that show the characteristically different features of the effective chemical potential μ and the cutoff Λ for two different types of mWSMs. We also narrate the key roles played by the topological charge n and the tilt C in the thermoelectric transport properties of mWSMs in its two counterparts. We note that dispersion becomes anisotropic due to the multi-Weyl nature; tilt can additionally make it anisotropic in the tilt direction. For mWSMs, the Fermi surface becomes a distorted circle or cone depending on the tilt in the static limit. The distribution of chiral Weyl fermions also takes part importantly in transport. Floquet driving can lead to further complicated deformation of the static Fermi surface. Moreover, it can influence the distribution of chiral Weyl fermions in the electron and hole pockets. Therefore, Floquet transport can noticeably be altered upon the introduction of the tilt. In terms of the physical parameters, the differences in transport are clearly visible, which originate from the nature of the Fermi surface. Having qualitatively analyzed the differences, we below present their quantitative nature.

It is to be noted that Λ^2 is associated with $\mu^{2M/n-4}$ and $\mu^{2M/n-5}$ (with $M = 1, 2$) for optical Hall conductivity and Nernst conductivity in the case of type-II mWSMs, respectively. Therefore, the transport properties in this phase are heavily influenced by the coupling of μ and Λ . This is contrary to the type-I mWSM where only μ can affect the transport in addition to the driving field; Λ does not appear

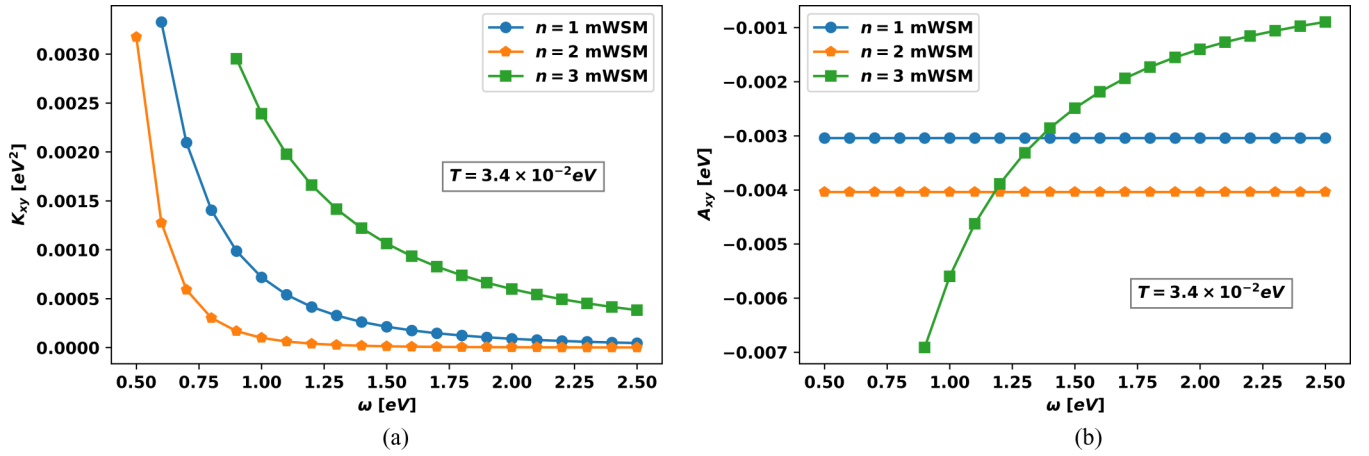


FIG. 1. Type-I WSM: (a) Variation of thermal anomalous Hall conductivity with optical frequency, for three different values of the monopole charge. (b) Variation of anomalous Nernst conductivity with optical frequency, for three different values of the monopole charge. The values of the various parameters are specified in natural units as follows: $v_F = 0.005$, $\alpha_1 = v_F$, $\alpha_2 = 0.00012$ eV⁻¹, $\alpha_3 = 0.00012$ eV⁻², $E_0 = \omega A_0 = 1000.0$ eV², $C = 0.1$, $\mu = 1.0$ eV, $Q = 2.0$ eV, and $T = 3.4 \times 10^{-2}$ K.

in the transport coefficients. For the type-II single WSM, a purely logarithmic cutoff dependence is only observed. Hence, the anisotropy in the tilted dispersion nontrivially couples with the field parameters to generate the unusual cutoff dependence. The shape of the Fermi pockets for type-II mWSMs is very different from type-I mWSM as is evident from the cutoff dependence of transport coefficients. Notably, in the case of irradiated tilted mWSMs, the topological charge imprints its effect not only in a simple multiplicative fashion but also in a much more fundamental way, by coupling to the tilt-dependent effective chemical potential, where Δ appears algebraically. This algebraic cutoff-dependent term is associated with the additional corrections of $O(1/\omega)$. The leading order term in the off-diagonal conductivity is given by n times the single-Weyl result; here, the anisotropic nature of the dispersion is partially encoded in the renormalized chemical potential $\mu \rightarrow \mu - C\Delta_n$, where $\Delta_n = O(A_0^{2n}/\omega)$. The effective chemical potential is also dependent on the frequency of the driving potential and the monopole charge.

Having discussed the implication of the cutoff, we here investigate the nonlinear μ dependence that arises in the conductivity tensor, besides the effective μ . In type-I mWSMs, considering $v \gg |C|$, the vacuum contribution σ_{xy}^I associated with the $\beta'_{2,3}$ term becomes a decreasing function of μ for both $n = 2$ and $n = 3$; the β'_2 term decays inversely (as μ^{-1}) for $n = 2$ and $\beta'_{2,(3)}$ decays nonlinearly $\mu^{-4/3}$ ($\mu^{-2/3}$) for $n = 3$. The Nernst conductivity on the other hand goes as μ^{-2} for $n = 2$ and for $n = 3$, it becomes a decreasing function of μ (as $\mu^{-7/3}$ and $\mu^{-5/3}$). In type-II mWSMs, considering $|C| \gg v$, the vacuum contribution σ_{xy}^{II} associated with the $\beta'_{2,3}\Lambda^2$ term becomes a decreasing function of μ for both the $n = 2$ and $n = 3$ cases. We note that the subleading correction decays more rapidly with μ for type-II as compared to type-I mWSMs. In particular, the cutoff-independent contributions associated with the β'_2 term vary as μ^{-2} and μ^{-3} for $n = 2$, while for $n = 3$, these contributions associated with the $\beta'_{2,(3)}$ term go as $\mu^{-7/3}$ and $\mu^{-10/3}$ ($\mu^{-5/3}$ and $\mu^{-8/3}$). The Nernst conductivity in this regime becomes a strongly decreasing

function of μ for both $n = 2$ and $n = 3$ with the lowest power as μ^{-3} and $\mu^{-8/3}$, respectively.

After investigating the transport behavior analytically, we below illustrate them as a function of driving frequency to analyze some salient qualitative features. We note that our aim is to pictorially differentiate the type-I from type-II mWSMs based on our low-energy model. Hence, at the outset, we confess that certain lattice effects might not be captured following our analysis. However, our study uncovers some trends which we believe can be probed in real materials.

We now discuss the transport coefficients for type-I mWSMs as shown in Fig. 1(a) for thermal Hall conductivity and Fig. 1(b) for Nernst conductivity. We here depict the high-frequency behavior of K_{xy} and α_{xy} , calculated using Eq. (33) and Eq. (34), respectively. Noticeably the response from the external field for a general $n > 1$ mWSM is not related to the $n = 1$ single WSM by a simple multiplicative factor. This is also very clearly evident from the variation of K_{xy} and α_{xy} with driving frequency ω . The subleading terms play an important role due to the fact that the chemical potential μ gets nontrivially coupled to the frequency; these terms are associated with the factors β'_2 , β'_3 . The important point to note here is that K_{xy} decreases and eventually saturates with optical frequency ω , while $|\alpha_{xy}|$ remains unchanged with ω for $n = 2$. In the case with $n = 3$, $|\alpha_{xy}|$ increases followed by a saturation at sufficiently large frequency. We note that even though $\beta''_2 = \beta''_3 = 0$ for both $n = 1$ and $n = 2$, K_{xy} depends on ω as the first two terms in Eq. (33) encompass the factor Δ_n . The ω -independent nature of $\alpha_{xy}^{n=1}$ and $\alpha_{xy}^{n=2}$ stems from the fact that $\beta''_2 = \beta''_3 = 0$ in the leading order; the first term in Eq. (34) does not depend on ω . $\beta''_2, \beta''_3 \neq 0$, which results in ω -dependent behavior of $\alpha_{xy}^{n=3}$. The absence and lower degree of anisotropy can thus lead to ω -independent nature of $\alpha_{xy}^{n=1}$ and $\alpha_{xy}^{n=2}$, respectively; a substantial amount of anisotropy can significantly modify the light-induced transport as observed in $\alpha_{xy}^{n=3}$. However, the crossing of $\alpha_{xy}^{n=3}$ with $\alpha_{xy}^{n=1}$ and $\alpha_{xy}^{n=2}$ might be restricted to the leading order, and higher-order correction can be frequency dependent, which we do not calculate here.

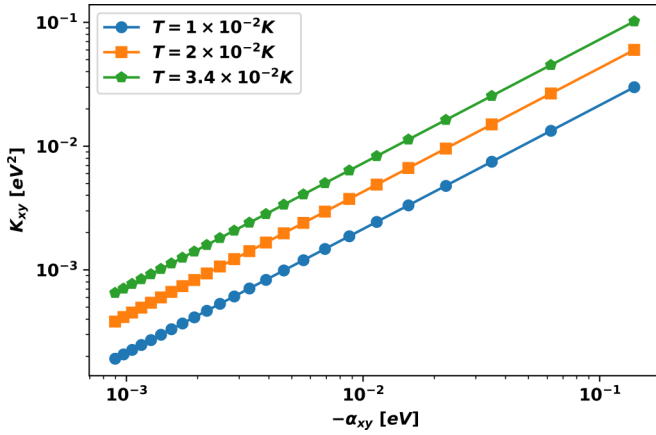


FIG. 2. Type-I WSM: Variation of thermal anomalous Hall conductivity with anomalous Nernst conductivity, for $n = 3$ mWSM. The frequency range sampled is 0.50 eV to 2.50 eV. The temperature values sampled are $T = 1 \times 10^{-2}, 2 \times 10^{-2}, 3.4 \times 10^{-2}$ K. The values of the other various parameters are the same as in Fig. 1.

We can comment that one needs to investigate the lattice model to get the complete picture.

It is now important to analyze the behavior of K_{xy} as a function of α_{xy} that could be useful from the experimental perspective. One can understand that K_{xy} and α_{xy} behave in an independent manner for $n = 1$ and 2 as K_{xy} depends on ω while α_{xy} does not. Interestingly, we see that this no longer holds for $n = 3$ and we plot this in Fig. 2. Here, K_{xy} increases with $|\alpha_{xy}|$. A qualitative change in the transport character is observed with the increase in the degree of anisotropy, characterized by n .

Similarly, for type-II mWSMs, we depict the behavior of K_{xy} , obtained from Eq. (36), in Fig. 3(a) and α_{xy} , obtained from Eq. (37), in Fig. 3(b). One can find here for the type-II mWSM, unlike the type-I mWSM, that K_{xy} and α_{xy} both decrease with ω . This may be due to the fact that they are influenced by the quadratic momentum cutoff Λ^2 dependent

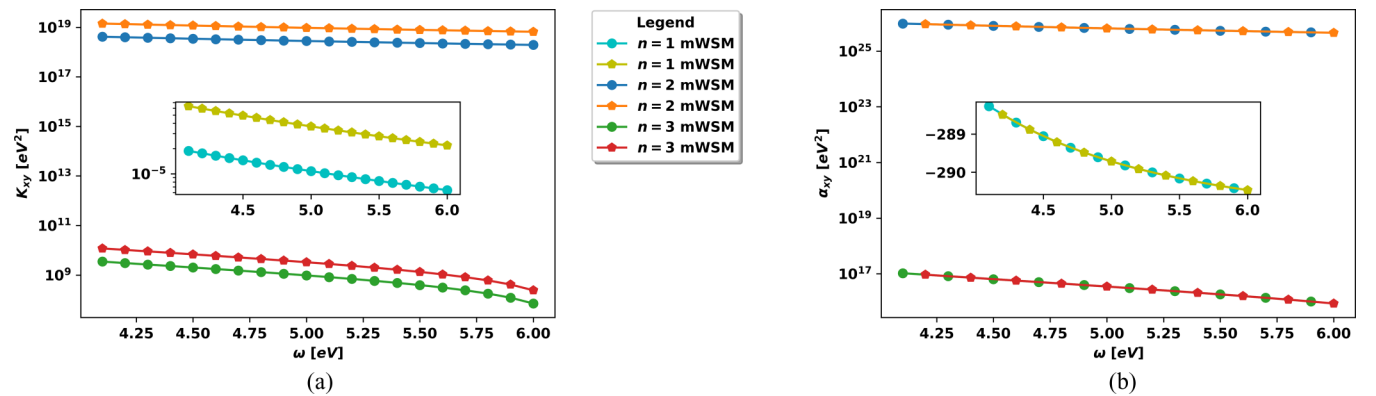


FIG. 3. Type-II WSM: (a) Variation of thermal anomalous Hall conductivity with optical frequency, for three different values of the monopole charge. (b) Variation of anomalous Nernst conductivity with optical frequency, for three different values of the monopole charge. The plot (b) shows a strong overlap between the curves for fixed n as a function of temperature. To highlight this issue, the data points sampled for overlapping curves are at distinct values of frequency. The values of the various parameters are specified in natural units as follows: $v_F = 0.005$, $\alpha_1 = v_F$, $\alpha_2 = 0.00012 \text{ eV}^{-1}$, $\alpha_3 = 0.00012 \text{ eV}^{-2}$, $E_0 = \omega A_0 = 1000.0 \text{ eV}^2$, $C = 0.1$, $\mu = 1.0 \text{ eV}$, $Q = 2.0 \text{ eV}$, $\Lambda = 900.0 \text{ eV}$, and $T = 1 \times 10^{-2}, 2 \times 10^{-2} \text{ K}$.

subleading term in addition to the terms containing the function $f(\mu, \omega, n)$. We note in the sufficiently large frequency regime that conductivities for type-I triple WSMs are at a higher magnitude as compared to single and double WSMs, while this is not the case for type II. The responses from type-II double WSMs acquire maximum value. For type I, conductivities of double WSMs become lowest in the sufficiently large frequency regime; in contrast, the conductivities for type-II single WSMs becomes vanishingly small as shown in the insets of Figs. 3(a) and 3(b). We note that α_{xy} behaves identically with temperature for type-II single WSMs and mWSMs as shown in Fig. 3(b). Having investigated anomalous thermal Hall and Nernst coefficients for a range of physically viable parameters such as ω , we show that type-I and type-II mWSMs can be qualitatively distinguished in terms of their transport behavior.

Now we shall focus on the role of the topological charge n in different transport properties. For that, we plot K_{xy} as a function of α_{xy} for $n = 2$ in Fig. 4(a), and for $n = 3$ in Fig. 4(b). It is known that K_{xy} and α_{xy} share a linear relationship [30] for $n = 1$, and we notice that this holds for $n = 2$: This can be attributed to the fact the first subleading order term remains small for a given chemical potential. This no longer holds for $n = 3$ as is evident from Fig. 4(b) where the subleading order terms play a crucial role. Therefore, one finds a qualitative change in the transport character with n , as the degree of anisotropy is enhanced. A comparison between Fig. 2 and Fig. 4(b) suggests that K_{xy} decreases with increasing $|\alpha_{xy}|$ for type II while K_{xy} increases with increasing $|\alpha_{xy}|$ for type I. Therefore, tilt can significantly modify the transport even for the irradiated mWSMs.

Having thoroughly investigated the transport coefficients of type-I and type-II mWSMs, we would now like to comment on the differences between these two phases in single WSMs as far as the other magnetotransport conductivities are concerned. As a start, planar Hall coefficients vary quadratically (linearly) for type-I (type-II) single WSMs [84]. The type-I single WSMs can be differentiated from type II while

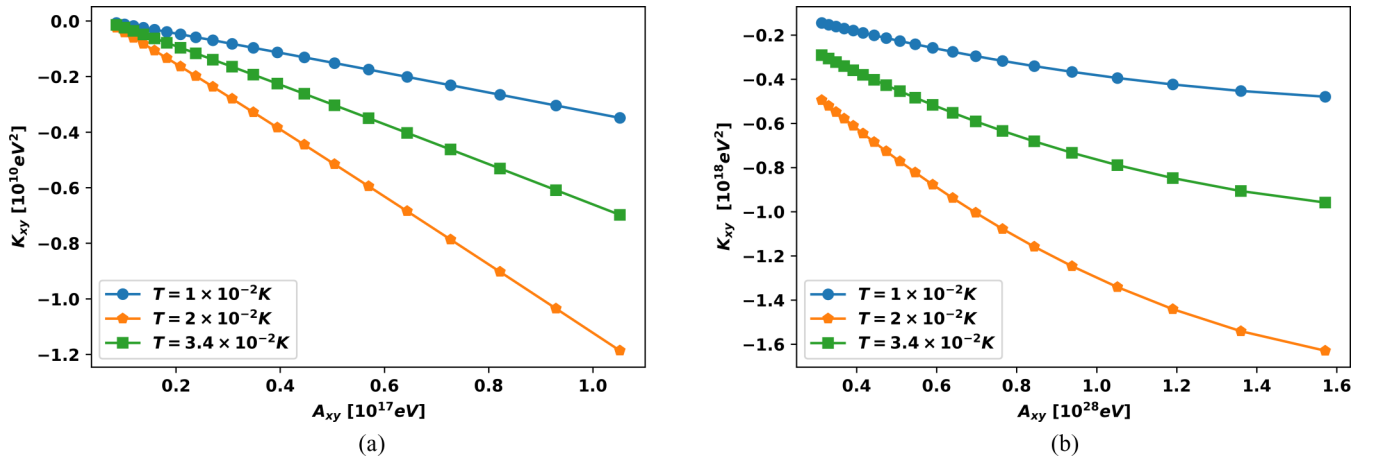


FIG. 4. Type-II WSM: (a) Variation of thermal anomalous Hall conductivity with anomalous Nernst conductivity, for $n = 2$ mWSM. (b) Variation of thermal anomalous Hall conductivity with anomalous Nernst conductivity, for $n = 3$ mWSM. For both cases, the frequency range sampled is 4.1 eV to 6 eV. The temperature values sampled are $T = 1 \times 10^{-2}$, 2×10^{-2} , 3.4×10^{-2} K. The values of the other various parameters are the same as in Fig. 3.

the anomalous Nernst and anomalous Hall conductivities are studied [85,86]. The tilt also causes distinguishably different optical activities in Kerr and Faraday rotation as compared to the nontilted case [50,87]. Our study considering the low-energy irradiated mWSM model further strengthens the list of distinction between these two types of mWSMs. The distinct behavior coming from type-I and type-II single-Weyl lattice models which do not suffer from any cutoff dependence can thus be related to the different cutoff characteristics as derived in the low-energy model. Therefore, the tilt even in the presence of anisotropy is able to influence the transport properties in a different manner as compared to the nontilted case.

We shall now propose a relevant experimental setup where our predictions can be tested. One can have candidate double (HgCr₂Se₄) and triple WSM [Rb(MoTe)₃] materials as the samples. The Floquet driving can be realized by the conventional pump (strong beam)–probe (weak beam) optical setup where ultrafast electron dynamics of the samples are observed as a function of time delay between the arrival of pump and probe pulses. Recently, using polarized photons at mid-infrared wavelengths, Floquet-Bloch states and photoinduced band gaps have been shown to be clearly visible in time-and-angle-resolved photoemission spectroscopy [88]. We believe that using similar arrangements with suitably chosen frequency ranges of pump laser, one can experimentally measure the transport properties derived here. One can also consider a nonoptical substrate-terminal-based closed circuit measurement of Nernst conductivity and thermal Hall conductivity [44]. The electric and heat current can be measured considering a mutually perpendicular arrangement of DC power source and thermocouple, respectively.

VI. CONCLUSION

In this paper we have investigated the circularly polarized light (of amplitude A_0 and frequency ω) induced contributions to the thermoelectric transport coefficients in type-I and type-II mWSMs with topological charge $n > 1$ considering the low-energy minimal model. Using the high-frequency ex-

pansion ($\omega \rightarrow \infty$) and appropriately employing the nonequilibrium Floquet-Kubo formalism, where the energies and states of the Hamiltonian are replaced by the quasienergy and quasistates of the effective Hamiltonian, we study the anomalous thermal Hall conductivity and Nernst conductivity. The effective Floquet Hamiltonian suggests that the Weyl nodes, separated by Q in the momentum space for the static case, are further displaced by a distance $2\Delta_n \sim A_0^{2n}/\omega$. Importantly, the low-energy Hamiltonian of Floquet mWSMs receives momentum-dependent corrections in addition to the constant A_0^2 shift in the single $n = 1$ Floquet WSMs. This results in a change in the effective Fermi surface which in turn leads to an array of nontrivial consequences for the transport coefficients. The leading order contribution varies linearly with the topological charge and the chemical potential μ is renormalized to $\mu - C\Delta_n$. Therefore, the light-induced transport phenomena in type-I and type-II mWSMs become significantly different. In particular, one can show that optical conductivity increases with A_0 for type-I mWSMs, while it decreases with A_0 in the case of type-II mWSMs. However, the leading order vacuum contribution to σ_{xy} remains topological, which we verify by calculating the Berry-curvature-induced anomalous Hall conductivity.

Going beyond the leading order contribution, we compute the effect of the momentum-dependent correction term in the Fermi surface effects to the conductivity tensor. We find that the Floquet-driving-induced subleading contribution can show nontrivial algebraic dependence on the chemical potential μ as $\mu^{f(n)}$. Most surprisingly, unlike the case of type-II single WSMs, for type-II mWSMs, the Nernst and thermal Hall conductivity depends algebraically on the momentum cutoff. However, for type-I mWSMs, the Fermi surface contribution remains cutoff independent. On the other hand, it decays slowly for type-I mWSMs as compared to type-II mWSMs. Consequently, unlike the type-I single WSMs, the Nernst conductivity for type-I mWSMs depends on μ . Combining all these, we graphically represent the variation of the total thermal Hall and Nernst conductivities as a function of the optical driving frequency by evaluating the analytical

expression numerically. These suggest that type-I and type-II mWSMs exhibit distinct behavior while the multi-Weyl nature can also be captured vividly. This would directly connect our study with possible future experiments. In conjunction with the previous point, we discuss the possible experimental measurements and setups of our analytical findings. Therefore, we believe that our work could motivate a plethora of studies

in the related experimental and theoretical areas dealing with driven WSMs.

ACKNOWLEDGMENTS

T.N. specially thanks MPIPES, Dresden, Germany, for providing local hospitality.

-
- [1] M. Z. Hasan, S.-Y. Xu, I. Beloposky, and S.-M. Huang, *Annu. Rev. Condens. Matter Phys.* **8**, 289 (2017).
- [2] N. P. Armitage, E. J. Mele, and A. Vishwanath, *Rev. Mod. Phys.* **90**, 015001 (2018).
- [3] X. Wan, A. M. Turner, A. Vishwanath, and S. Y. Savrasov, *Phys. Rev. B* **83**, 205101 (2011).
- [4] T. M. McCormick, I. Kimchi, and N. Trivedi, *Phys. Rev. B* **95**, 075133 (2017).
- [5] A. A. Zyuzin, S. Wu, and A. A. Burkov, *Phys. Rev. B* **85**, 165110 (2012).
- [6] U. Dey, S. Nandy, and A. Taraphder, *Sci. Rep.* **10**, 2699 (2020).
- [7] A. A. Zyuzin and A. A. Burkov, *Phys. Rev. B* **86**, 115133 (2012).
- [8] D. T. Son and B. Z. Spivak, *Phys. Rev. B* **88**, 104412 (2013).
- [9] A. A. Burkov, *J. Phys.: Condens. Matter* **27**, 113201 (2015).
- [10] S.-Y. Xu *et al.*, *Science* **349**, 613 (2015).
- [11] B. Lv, *Nat. Phys.* **11**, 724 (2015).
- [12] B. Lv, *Phys. Rev. X* **5**, 031013 (2015).
- [13] G. Xu, H. Weng, Z. Wang, X. Dai, and Z. Fang, *Phys. Rev. Lett.* **107**, 186806 (2011).
- [14] C. Fang, M. J. Gilbert, X. Dai, and B. A. Bernevig, *Phys. Rev. Lett.* **108**, 266802 (2012).
- [15] B.-J. Yang and N. Nagaosa, *Nat. Commun.* **5**, 4898 (2014).
- [16] E. McCann and V. I. Fal'ko, *Phys. Rev. Lett.* **96**, 086805 (2006).
- [17] F. Guinea, A. H. Castro Neto, and N. M. R. Peres, *Phys. Rev. B* **73**, 245426 (2006).
- [18] H. Min and A. H. MacDonald, *Phys. Rev. B* **77**, 155416 (2008).
- [19] S. Park, S. Woo, E. J. Mele, and H. Min, *Phys. Rev. B* **95**, 161113(R) (2017).
- [20] E. V. Gorbar, V. A. Miransky, I. A. Shovkovy, and P. O. Sukhachov, *Phys. Rev. B* **96**, 155138 (2017).
- [21] R. M. A. Dantas, F. Pena-Benitez, B. Roy, and P. Surowka, *J. High Energy Phys.* **12** (2018) 069.
- [22] L. Lepori, M. Burrello, and E. Guadagnini, *J. High Energy Phys.* **06** (2018) 110.
- [23] T. Nag and S. Nandy, [arXiv:1812.08322](https://arxiv.org/abs/1812.08322).
- [24] D. Sinha and K. Sengupta, *Phys. Rev. B* **99**, 075153 (2019).
- [25] R. M. A. Dantas, F. Peña-Benitez, B. Roy, and P. Surowka, *Phys. Rev. Research* **2**, 013007 (2020).
- [26] B. Yan and C. Felser, *Annu. Rev. Condens. Matter Phys.* **8**, 337 (2017).
- [27] G. Volovik and M. Zubkov, *Nucl. Phys. B* **881**, 514 (2014).
- [28] Y. Xu, F. Zhang, and C. Zhang, *Phys. Rev. Lett.* **115**, 265304 (2015).
- [29] A. A. Soluyanov, D. Gresch, Z. Wang, Q. Wu, M. Troyer, X. Dai, and B. A. Bernevig, *Nature (London)* **527**, 495 (2015).
- [30] A. Menon, D. Chowdhury, and B. Basu, *Phys. Rev. B* **98**, 205109 (2018).
- [31] P. Li, Y. Wen, X. He, Q. Zhang, C. Xia, Z.-M. Yu, S. A. Yang, Z. Zhu, H. N. Alshareef, and X.-X. Zhang, *Nat. Commun.* **8**, 2150 (2017).
- [32] S.-i. Kimura, Y. Nakajima, Z. Mita, R. Jha, R. Higashinaka, T. D. Matsuda, and Y. Aoki, *Phys. Rev. B* **99**, 195203 (2019).
- [33] M. Trescher, B. Sviderski, P. W. Brouwer, and E. J. Bergholtz, *Phys. Rev. B* **91**, 115135 (2015).
- [34] F. Fei, X. Bo, R. Wang, B. Wu, J. Jiang, D. Fu, M. Gao, H. Zheng, Y. Chen, X. Wang, H. Bu, Fengqi Song, X. Wan, B. Wang, and G. Wang, *Phys. Rev. B* **96**, 041201(R) (2017).
- [35] Z.-M. Yu, Y. Yao, and S. A. Yang, *Phys. Rev. Lett.* **117**, 077202 (2016).
- [36] M. Udagawa and E. J. Bergholtz, *Phys. Rev. Lett.* **117**, 086401 (2016).
- [37] Y.-Y. Lv, *Phys. Rev. Lett.* **118**, 096603 (2017).
- [38] K. Landsteiner, *Phys. Rev. B* **89**, 075124 (2014).
- [39] G. Sharma, P. Goswami, and S. Tewari, *Phys. Rev. B* **93**, 035116 (2016).
- [40] A. Lucas, R. A. Davison, and S. Sachdev, *Proc. Natl. Acad. Sci. USA* **113**, 9463 (2016).
- [41] Q. Chen and G. A. Fiete, *Phys. Rev. B* **93**, 155125 (2016).
- [42] F. C. Chen, H. Y. Lv, X. Luo, W. J. Lu, Q. L. Pei, G. T. Lin, Y. Y. Han, X. B. Zhu, W. H. Song, and Y. P. Sun, *Phys. Rev. B* **94**, 235154 (2016).
- [43] M. Hirschberger, S. Kushwaha, Z. Wang, Q. Gibson, S. Liang, C. A. Belvin, B. A. Bernevig, R. J. Cava, and N. P. Ong, *Nat. Mater.* **15**, 1161 (2016).
- [44] S. J. Watzman, T. M. McCormick, C. Shekhar, S.-C. Wu, Y. Sun, A. Prakash, C. Felser, N. Trivedi, and J. P. Heremans, *Phys. Rev. B* **97**, 161404(R) (2018).
- [45] U. Stocker *et al.*, *J. Phys.: Condens. Matter* **29**, 325701 (2017).
- [46] C. J. Tabert and J. P. Carbotte, *Phys. Rev. B* **93**, 085442 (2016).
- [47] S. P. Mukherjee and J. P. Carbotte, *Phys. Rev. B* **97**, 045150 (2018).
- [48] S. P. Mukherjee and J. P. Carbotte, *Phys. Rev. B* **96**, 085114 (2017).
- [49] C. J. Tabert, J. P. Carbotte, and E. J. Nicol, *Phys. Rev. B* **93**, 085426 (2016).
- [50] K. Sonowal, A. Singh, and A. Agarwal, *Phys. Rev. B* **100**, 085436 (2019).
- [51] K. Das and A. Agarwal, *Phys. Rev. B* **100**, 085406 (2019).
- [52] S.-M. Huang *et al.*, *Proc. Natl. Acad. Sci. USA* **113**, 1180 (2016).
- [53] Q. Liu and A. Zunger, *Phys. Rev. X* **7**, 021019 (2017).
- [54] T. Oka and H. Aoki, *Phys. Rev. B* **79**, 081406(R) (2009).
- [55] T. Kitagawa, E. Berg, M. Rudner, and E. Demler, *Phys. Rev. B* **82**, 235114 (2010).
- [56] M. S. Rudner, N. H. Lindner, E. Berg, and M. Levin, *Phys. Rev. X* **3**, 031005 (2013).
- [57] F. Nathan and M. S. Rudner, *New J. Phys.* **17**, 125014 (2015).
- [58] P. Titum, E. Berg, M. S. Rudner, G. Refael, and N. H. Lindner, *Phys. Rev. X* **6**, 021013 (2016).

- [59] H. C. Po, L. Fidkowski, T. Morimoto, A. C. Potter, and A. Vishwanath, *Phys. Rev. X* **6**, 041070 (2016).
- [60] S. Kar and B. Basu, *Phys. Rev. B* **98**, 245119 (2018).
- [61] A. Das, *Phys. Rev. B* **82**, 172402 (2010).
- [62] L. D'Alessio and A. Polkovnikov, *Ann. Phys. (NY)* **333**, 19 (2013).
- [63] T. Nag, S. Roy, A. Dutta, and D. Sen, *Phys. Rev. B* **89**, 165425 (2014).
- [64] A. Agarwala, U. Bhattacharya, A. Dutta, and D. Sen, *Phys. Rev. B* **93**, 174301 (2016); A. Agarwala and D. Sen, *ibid.* **95**, 014305 (2017).
- [65] T. Nag, V. Juricic, and B. Roy, *Phys. Rev. Res.* **1**, 032045 (2019).
- [66] M. Thakurathi, A. A. Patel, D. Sen, and A. Dutta, *Phys. Rev. B* **88**, 155133 (2013).
- [67] H. Hubener, M. A. Sentef, U. De Giovannini, A. F. Kemper, and A. Rubio, *Nat. Commun.* **8**, 13940 (2017).
- [68] Z. Gu, H. A. Fertig, D. P. Arovas, and A. Auerbach, *Phys. Rev. Lett.* **107**, 216601 (2011).
- [69] X-X. Zhang, T. T. Ong, and N. Nagaosa, *Phys. Rev. B* **94**, 235137 (2016).
- [70] Z. Yan and Z. Wang, *Phys. Rev. Lett.* **117**, 087402 (2016).
- [71] N. Goldman and J. Dalibard, *Phys. Rev. X* **4**, 031027 (2014).
- [72] T. Mikami *et al.*, *Phys. Rev. B* **93**, 144307 (2016).
- [73] S. Ahn, E. J. Mele, and H. Min, *Phys. Rev. B* **95**, 161112(R) (2017); B. Roy, P. Goswami, and V. Juricic, *ibid.* **95**, 201102(R) (2017).
- [74] See Supplemental Material at <http://link.aps.org/supplemental/10.1103/PhysRevB.102.014307> for brief discussion on multi-Weyl lattice model, Floquet dispersion, current operator and Floquet Kubo formalism.
- [75] J. H. Shirley, *Phys. Rev.* **138**, B979 (1968).
- [76] J. C. Sandoval-Santana *et al.*, *Ann. Phys.* **531**, 1900035 (2019).
- [77] X-L. Qi, Y-S. Wu, and S-C. Zhang, *Phys. Rev. B* **74**, 085308 (2006).
- [78] L. Bucciantini, S. Roy, S. Kitamura, and T. Oka, *Phys. Rev. B* **96**, 041126(R) (2017).
- [79] M. Wackerl, P. Wenk, and J. Schliemann, *Phys. Rev. B* **101**, 184204 (2020); A. Kumar, M. Rodriguez-Vega, T. Pereg-Barnea, and B. Seradjeh, *ibid.* **101**, 174314 (2020); H. Dehghani, T. Oka, and A. Mitra, *ibid.* **91**, 155422 (2015); H. Dehghani and A. Mitra, *ibid.* **92**, 165111 (2015).
- [80] J. M. Luttinger, *Phys. Rev.* **135**, A1505 (1964).
- [81] Yago Ferreira, A. A. Zyuzin, and Jens H. Bardarson, *Phys. Rev. B* **96**, 115202 (2017).
- [82] R. Lundgren, P. Laurell, and G. A. Fiete, *Phys. Rev. B* **90**, 165115 (2014).
- [83] M. Jonson and G. D. Mahan, *Phys. Rev. B* **21**, 4223 (1980).
- [84] S. Nandy, G. Sharma, A. Taraphder, and S. Tewari, *Phys. Rev. Lett.* **119**, 176804 (2017).
- [85] S. Saha and S. Tewari, *Eur. Phys. J. B* **91**, 4 (2018).
- [86] G. Sharma, P. Goswami, and S. Tewari, *Phys. Rev. B* **96**, 045112 (2017).
- [87] M. Kargarian, M. Randeria, and N. Trivedi, *Sci. Rep.* **5**, 12683 (2015).
- [88] H. Wang, H. Steinberg, P. Jarillo-Herrero, and N. Gedik, *Science* **342**, 453 (2013).